# The two-component afterglow of *Swift* GRB 050802

S. R. Oates,[1]★ M. De Pasquale,[1] M. J. Page,[1] A. J. Blustin,[1] S. Zane,[1] K. McGowan,[2]
K. O. Mason,[1] T. S. Poole,[1] P. Schady,[1] P. W. A. Roming,[3] K. L. Page,[4] A. Falcone[3]
and N. Gehrels[5]

[1]*Mullard Space Science Laboratory, University College London, Holmbury St Mary, Dorking, Surrey RH5 6NT*
[2]*School of Physics and Astronomy, University of Southampton, Highfield, Southampton SO17 1BJ*
[3]*Department of Astronomy and Astrophysics, Pennsylvania State University, 525 Davey Laboratory, University Park, PA 16802, USA*
[4]*Department of Physics and Astronomy, University of Leicester, University Road, Leicester LE1 7RH*
[5]*NASA Goddard Space Flight Center, Laboratory for High Energy Astrophysics, Greenbelt, MD 20771, USA*

**ABSTRACT**

This paper investigates GRB 050802, one of the best examples of a *Swift* gamma-ray burst afterglow that shows a break in the X-ray light curve, while the optical counterpart decays as a single power law. This burst has an optically bright afterglow of 16.5 mag, detected throughout the 170–650 nm spectral range of the Ultraviolet and Optical Telescope (UVOT) onboard *Swift*. Observations began with the X-ray Telescope and UVOT telescopes 286 s after the initial trigger and continued for $1.2 \times 10^6$ s. The X-ray light curve consists of three power-law segments: a rise until 420 s, followed by a slow decay with $\alpha = 0.63 \pm 0.03$ until 5000 s, after which, the light curve decays faster with a slope of $\alpha_3 = 1.59 \pm 0.03$. The optical light curve decays as a single power law with $\alpha_O = 0.82 \pm 0.03$ throughout the observation. The X-ray data on their own are consistent with the break at 5000 s being due to the end of energy injection. Modelling the optical to X-ray spectral energy distribution, we find that the optical afterglow cannot be produced by the same component as the X-ray emission at late times, ruling out a single-component afterglow. We therefore considered two-component jet models and find that the X-ray and optical emission is best reproduced by a model in which both components are energy injected for the duration of the observed afterglow and the X-ray break at 5000 s is due to a jet break in the narrow component. This bright, well-observed burst is likely a guide for interpreting the surprising finding of *Swift* that bursts seldom display achromatic jet breaks.

**Key words:** gamma-rays: bursts.

## 1 INTRODUCTION

Gamma-ray bursts (GRBs) are the most energetic explosions that take place in our Universe, with a typical energy of $10^{51}$–$10^{53}$ erg released on a time-scale of between a millisecond and a few thousand seconds. The release of such a considerable amount of energy over such a short period requires an outflow that is relativistic (Mészáros & Rees 1997a) and is likely to be anisotropic (Sari, Piran & Helpen 1999). The energy within the outflow is released primarily though shocks. The GRB is thought to be produced through internal shocks from interactions between successive shells of ejecta (Sari & Piran 1997). Subsequently an afterglow is emitted as the outflow is decelerated through collisionless shocks with the external medium (Sari 1997). A forward shock propagates into the external medium and emits from X-ray to radio wavelengths, and a reverse shock travels back through the ejecta and peaks at longer wavelengths than the forward shock (Zhang et al. 2005).

The afterglow can reveal many properties of the progenitor and its surroundings. Currently, the most up to date model (Zhang et al. 2005) allows the use of the temporal and spectral indices to indicate the nature of the surrounding medium, whether it is a uniform-density medium, or a medium with a density that is decreasing radially as expected for a stellar wind, for example, $n \propto r^{-2}$, where $n$ is the particle density and $r$ is the radius from the GRB. The indices also indicate the location of the observing band relative to the synchrotron self-absorption frequency $\nu_a$, the peak frequency $\nu_m$ and cooling frequency $\nu_c$.

Some GRB afterglows have a period of slow decline in their light curves [$F(t) \propto t^{-\alpha}$, where $\alpha \sim 0.5$] (Zhang et al. 2005), which is generally accepted to be due to continued energy injection (Rees & Mészáros 1998). This energy could be due to a central engine that is long lasting (Dai & Lu 1998a; Zhang & Mészáros 2001), later shells catching up and colliding with slower shells that were emitted

★E-mail: sro@mssl.ucl.ac.uk

earlier (Rees & Mészáros 1998), or the slow release of energy stored in the form of Poynting flux (Zhang & Kobayashi 2005). The end of energy injection is signalled by an increase in decay rates of the afterglow light curves to $F(t) \propto t^{-\alpha}$, where $\alpha \sim 1$.

Currently, the most effective observatory for studying GRBs and their early afterglows is *Swift*, which has now been in operation for over two years. It has the ability to observe emission ranging from $\gamma$-rays to optical with the three onboard telescopes, namely, the Burst Alert Telescope (BAT; Barthelmy et al. 2005), the X-ray Telescope (XRT; Burrows et al. 2005a) and the Ultraviolet and Optical Telescope (UVOT; Roming et al. 2005). The BAT covers a large area of the sky allowing of the order of 100 bursts to be detected per year. When the BAT has been triggered by the GRB, the satellite slews automatically allowing the XRT and the UVOT to begin observing as soon as possible, usually within 100 s of the burst trigger. *Swift* is thus able to observe both the initial $\gamma$-ray explosion and the following early afterglow.

This paper looks at GRB 050802, a burst that appears to challenge the standard picture. At the end of the shallow decay the X-ray afterglow breaks to a steeper decay, while the optical afterglow continues to decay as a power law without a break. If both the X-ray and optical arise from the same component and if the X-ray break were due to the end of energy injection then the optical light curve would be expected to break at the same time. Such behaviour has been noted recently in six *Swift* GRB afterglows (Panaitescu et al. 2006a) of which GRB 050802 is currently the best example. This burst has an X-ray light curve with two distinct breaks and it was observed for $1.2 \times 10^6$ s. It also had an optically bright afterglow ($\sim$16 mag at early times) that was well sampled in six filters of the UVOT up to $1 \times 10^5$ s and thereafter observed with the white UVOT filter. In this paper we discuss the possible models that could explain this behaviour. We will use the convention flux $F = t^{-\alpha} \nu^{-\beta}$ with $\alpha$ and $\beta$ being the temporal and spectral indices, respectively. We assume the Hubble parameter $H_0 = 70 \, \mathrm{km \, s^{-1} \, Mpc^{-1}}$ and density parameters $\Omega_\Lambda = 0.7$ and $\Omega_\mathrm{m} = 0.3$. Uncertainties are quoted at $1\sigma$ unless otherwise stated.

## 2 *Swift* AND GROUND-BASED OBSERVATIONS

The BAT was triggered by GRB 050802 at 10:08:02 UT on 2005 August 2 (Band et al. 2005). The light curve rises for 5 s to the first of three peaks and has a $T_{90} = (13 \pm 2)$ s (90 per cent confidence level). The fluence in the 15–350 keV band is $(2.8 \pm 0.1) \times 10^{-6} \, \mathrm{erg \, cm^{-2}}$ to 90 per cent confidence level (Palmer et al. 2005). Observations with the XRT and UVOT began 289 and 286 s, respectively, after the BAT trigger (Band et al. 2005; McGowan et al. 2005a). Both the XRT and UVOT continued to observe until $1.2 \times 10^6$ s after the burst trigger.

The XRT began observations by locating the burst with image mode. After the burst was located, data were taken in windowed timing (WT) mode for 163 s. A fading uncatalogued source was found within 8 arcsec of the BAT position (Band et al. 2005) and was confirmed as the X-ray counterpart of GRB 050802. 480 s after the burst trigger, the XRT changed modes and continued observations in photon counting (PC) mode.

UVOT observations showed a fading, uncatalogued source at RA $= 14^\mathrm{h}37^\mathrm{m}05\overset{s}{.}69$, Dec. $= 27°47'12\overset{''}{.}2$ (McGowan et al. 2005a). Following the trigger, a series of automated exposures were taken in the three optical and three ultraviolet (UV) filters. A log of the observations is given in Table 1. The observations consisted of an initial 100-s 'finding chart' exposure in the $V$ band, 10-s exposures in each passband for seven rotations of the filter wheel, followed

by a sequence of $\sim$100- and $\sim$900-s exposures. Later observations (after $1 \times 10^5$ s), were taken in the UVOT white filter.

The afterglow was also imaged and detected with the 2.6-m Shain Telescope, 8 h after the burst, with $R$- and $i'$-band magnitudes of 20.6 and 20.2, respectively (Pavlenko et al. 2005). Spectroscopic observations were carried out with ALFOSC on the Nordic Optical Telescope. Several absorption features were detected providing a redshift measurement of $z = 1.71$ (Fynbo et al. 2005a,b). Fynbo et al. (2005a) discovered an extended source within 1 arcsec of the UVOT afterglow location, which they propose could be the host galaxy.

## 3 XRT AND UVOT DATA REDUCTION

### 3.1 X-ray data

The XRT data were reduced using the XRT pipeline software V2.0. Source and background counts were taken from the cleaned event files using extraction regions, in order to construct spectra and light curves. Events of grade 0–2 were used for the WT mode and 0–12 were used for the PC mode. For the WT mode data we used a 40-pixel strip for the source extraction region and a 40-pixel strip for the background extraction region. In the PC mode data the first 2.5 ks of data were found to be piled up and so required the use of an annular extraction region. The size of the region that was affected by pile-up was determined by comparing the radial profile of the afterglow with a model of the XRT point spread function (PSF). The radial profile and the model PSF are inconsistent at radii less than 2.5 pixel (6 arcsec), so we used an inner radius of 2.5 pixel and an outer radius of 30 pixel (71 arcsec). The size of the source extraction region for the rest of the PC data was 30 pixel (71 arcsec) radius. For all PC data, background counts were extracted from a circular region of radius 80 pixel (189 arcsec). Appropriate response matrices (RMs) were taken from the *Swift* calibration data base, CALDB 20060424 and effective area files were constructed using the standard XRT software. A correction factor was calculated and applied to the piled-up section of the XRT light curve to account for the excluded, piled up pixels. Fortunately, the source was not located near the bad pixel columns and so no correction was required.

### 3.2 UVOT data

The UVOT event files were screened for bad times (e.g. South Atlantic Anomaly passage, Earth-limb avoidance) and the images were corrected for Mod-8 noise using the standard UVOT software. The images were transformed to sky coordinates and then corrected for the $\sim$ 5 arcsec uncertainty in the aspect of the spacecraft pointing using BESPOKE software.

Counts for the afterglow were extracted using an aperture of radius 4 arcsec for the optical filters and 5 arcsec for the UV filters. Background subtraction was performed using counts extracted from a larger region offset from the source position. The measured count rates were aperture-corrected to radii of 6 arcsec for the $V$, $B$ and $U$ filters and 12 arcsec for the UV filters. These were then translated to magnitudes using the standard UVOT zero-points (see Table 1).

The optical light curve is shown in Fig. 1. The light curve from each filter of the UVOT was normalized to the $V$ filter. The normalization factor for each filter (see Table 2) was calculated by taking the average count rate through the filter in the 400–1000 s time range, and dividing this value by the average count rate in the $V$ filter over the same time interval. Later observations were obtained with the UVOT white filter; these were normalized to the

**Table 1.** UVOT observations of GRB 050802 given in (aperture-corrected) count rates and magnitudes. Count rates were aperture-corrected to 6 arcsec for $V$, $B$ and $U$ filters and to 12 arcsec for $UVW1$, $UVM2$ and $UVW2$ filters to enable the use of the UVOT zero-points to convert the count rates to magnitudes. The zero-points are $V = 17.83 \pm 0.09$, $B = 19.12 \pm 0.12$, $U = 18.34 \pm 0.23$, $UVW1 = 17.82 \pm 0.02$, $UVM2 = 17.19 \pm 0.23$, $UVW2 = 17.82 \pm 0.02$, white $= 19.78 \pm 0.02$.

| Filter | $T_{\text{Mid}}$ (s) | Exposure | Count rate | Magnitude | Filter | $T_{\text{Mid}}$ (s) | Exposure | Count rate | Magnitude |
|---|---|---|---|---|---|---|---|---|---|
| V | 291 | 10 | 3.5 ±0.8 | $16.5^{+0.3}_{-0.2}$ | UVW1 | 578 | 10 | 0.55 ±0.36 | $18.5^{+1.2}_{-0.6}$ |
| V | 301 | 10 | 1.8 ±0.7 | $17.2^{+0.5}_{-0.4}$ | UVW1 | 662 | 10 | 0.76 ±0.39 | $18.1^{+0.8}_{-0.4}$ |
| V | 311 | 10 | 1.7 ±0.7 | $17.2^{+0.6}_{-0.4}$ | UVW1 | 747 | 10 | 0.97 ±0.42 | $17.9^{+0.6}_{-0.4}$ |
| V | 321 | 10 | 3.3 ±0.8 | $16.5^{+0.3}_{-0.2}$ | UVW1 | 831 | 10 | 0.26 ±0.26 | $19.3^{+4.5}_{-0.7}$ |
| V | 331 | 10 | 0.98 ±0.60 | $17.9^{+1.0}_{-0.5}$ | UVW1 | 915 | 10 | 0.40 ±0.29 | $18.8^{+1.4}_{-0.6}$ |
| V | 341 | 10 | 2.7 ±0.8 | $16.8^{+0.3}_{-0.3}$ | UVW1 | 1045 | 100 | 0.44 ±0.09 | $18.7^{+0.3}_{-0.2}$ |
| V | 351 | 10 | 1.9 ±0.7 | $17.1^{+0.5}_{-0.3}$ | UVW1 | 1671 | 100 | 0.52 ±0.10 | $18.5^{+0.2}_{-0.2}$ |
| V | 361 | 10 | 3.0 ±0.8 | $16.6^{+0.3}_{-0.3}$ | UVW1 | 2296 | 100 | 0.21 ±0.07 | $19.5^{+0.5}_{-0.3}$ |
| V | 371 | 10 | 2.1 ±0.7 | $17.0^{+0.4}_{-0.3}$ | UVW1 | 2905 | 66 | 0.10 ±0.08 | $20.3^{+1.7}_{-0.6}$ |
| V | 381 | 10 | 2.6 ±0.7 | $16.8^{+0.4}_{-0.3}$ | UVW1 | 14220 | 578 | 0.079 ±0.026 | $20.6^{+0.4}_{-0.3}$ |
| V | 466 | 10 | 2.2 ±0.7 | $17.0^{+0.4}_{-0.3}$ | UVW1 | 31454 | 823 | 0.041 ±0.020 | $21.3^{+0.7}_{-0.4}$ |
| V | 550 | 10 | 1.1 ±0.6 | $17.8^{+0.9}_{-0.5}$ | UVW1 | 43037 | 796 | 0.005 ±0.019 | $>20.8 (3\sigma)$ |
| V | 634 | 10 | 0.93 ±0.57 | $17.9^{+1.0}_{-0.5}$ | UVW1 | 54604 | 803 | 0.012 ±0.020 | $>20.7 (3\sigma)$ |
| V | 718 | 10 | 2.4 ±0.7 | $16.9^{+0.4}_{-0.3}$ | UVM2 | 395 | 10 | −0.054 ±0.130 | $>18.4 (3\sigma)$ |
| V | 803 | 10 | 0.91 ±0.49 | $17.9^{+0.8}_{-0.5}$ | UVM2 | 480 | 10 | 0.19 ±0.18 | $19.0^{+3.2}_{-0.7}$ |
| V | 888 | 10 | 2.0 ±0.6 | $17.1^{+0.4}_{-0.3}$ | UVM2 | 564 | 10 | 0.073 ±0.130 | $>18.0 (3\sigma)$ |
| V | 972 | 10 | 0.76 ±0.44 | $18.1^{+0.9}_{-0.5}$ | UVM2 | 648 | 10 | 0.16 ±0.18 | $>17.6 (3\sigma)$ |
| V | 1464 | 10 | 0.90 ±0.14 | $17.9^{+0.2}_{-0.2}$ | UVM2 | 732 | 10 | 0.33 ±0.22 | $18.4^{+1.1}_{-0.5}$ |
| V | 2088 | 10 | 0.53 ±0.12 | $18.5^{+0.3}_{-0.2}$ | UVM2 | 817 | 10 | −0.055 ±0.130 | $>18.4 (3\sigma)$ |
| V | 2714 | 100 | 0.33 ±0.11 | $19.0^{+0.5}_{-0.3}$ | UVM2 | 901 | 10 | 0.056 ±0.130 | $>18.1 (3\sigma)$ |
| V | 12566 | 100 | 0.11 ±0.04 | $20.2^{+0.5}_{-0.3}$ | UVM2 | 986 | 10 | −0.055 ±0.130 | $>18.4 (3\sigma)$ |
| V | 25528 | 100 | 0.028 ±0.032 | $>20.1 (3\sigma)$ | UVM2 | 1567 | 100 | 0.073 ±0.041 | $20.0^{+0.9}_{-0.5}$ |
| V | 41283 | 900 | −0.044 ±0.041 | $>20.6 (3\sigma)$ | UVM2 | 2192 | 100 | 0.0051 ±0.0284 | $>19.8 (3\sigma)$ |
| V | 52838 | 900 | 0.055 ±0.041 | $21.0^{+1.4}_{-0.6}$ | UVM2 | 2818 | 100 | 0.038 ±0.038 | $>19.2 (3\sigma)$ |
| B | 437 | 10 | 4.6 ±1.0 | $17.5^{+0.3}_{-0.2}$ | UVM2 | 13473 | 900 | 0.021 ±0.010 | $21.4^{+0.7}_{-0.4}$ |
| B | 521 | 10 | 3.3 ±0.9 | $17.8^{+0.3}_{-0.3}$ | UVM2 | 26032 | 95 | −0.019 ±0.024 | $>20.4 (3\sigma)$ |
| B | 605 | 10 | 2.8 ±0.9 | $18.0^{+0.4}_{-0.3}$ | UVM2 | 30585 | 900 | 0.004 ±0.009 | $>20.9 (3\sigma)$ |
| B | 690 | 10 | 3.4 ±0.9 | $17.8^{+0.3}_{-0.2}$ | UVM2 | 42188 | 898 | −0.005 ±0.009 | $>21.4 (3\sigma)$ |
| B | 774 | 10 | 4.1 ±0.9 | $17.6^{+0.3}_{-0.2}$ | UVM2 | 53461 | 861 | 0.004 ±0.010 | $>20.8 (3\sigma)$ |
| B | 859 | 10 | 4.3 ±0.9 | $17.5^{+0.2}_{-0.2}$ | UVW2 | 452 | 10 | −0.151 ±0.133 | $>19.3 (3\sigma)$ |
| B | 943 | 10 | 3.7 ±0.8 | $17.7^{+0.3}_{-0.2}$ | UVW2 | 537 | 10 | 0.329 ±0.273 | $19.0^{+1.9}_{-0.7}$ |
| B | 1254 | 100 | 1.9 ±0.2 | $18.4^{+0.1}_{-0.1}$ | UVW2 | 621 | 10 | 0.023 ±0.137 | $>18.7 (3\sigma)$ |
| B | 1879 | 100 | 1.5 ±0.2 | $18.7^{+0.1}_{-0.1}$ | UVW2 | 705 | 10 | −0.036 ±0.134 | $>18.9 (3\sigma)$ |
| B | 2505 | 100 | 0.80 ±0.16 | $19.4^{+0.2}_{-0.2}$ | UVW2 | 790 | 10 | 0.26 ±0.22 | $19.3^{+2.2}_{-0.7}$ |
| B | 7631 | 900 | 0.38 ±0.05 | $20.2^{+0.1}_{-0.1}$ | UVW2 | 874 | 10 | 0.40 ±0.26 | $18.8^{+1.1}_{-0.5}$ |
| B | 36405 | 900 | 0.20 ±0.05 | $20.9^{+0.3}_{-0.2}$ | UVW2 | 958 | 10 | 0.028 ±0.13 | $>18.8 (3\sigma)$ |
| B | 47974 | 900 | 0.085 ±0.043 | $21.8^{+0.8}_{-0.4}$ | UVW2 | 1359 | 100 | 0.036 ±0.038 | $>19.9 (3\sigma)$ |
| U | 423 | 10 | 4.2 ±0.8 | $16.8^{+0.2}_{-0.2}$ | UVW2 | 1984 | 100 | 0.039 ±0.043 | $>19.8 (3\sigma)$ |
| U | 507 | 10 | 4.7 ±0.9 | $16.7^{+0.2}_{-0.2}$ | UVW2 | 2610 | 100 | 0.063 ±0.043 | $20.8^{+1.2}_{-0.6}$ |
| U | 591 | 10 | 2.3 ±0.7 | $17.5^{+0.4}_{-0.3}$ | UVW2 | 8406 | 634 | 0.028 ±0.015 | $21.7^{+0.8}_{-0.5}$ |
| U | 675 | 10 | 3.3 ±0.8 | $17.0^{+0.3}_{-0.2}$ | UVW2 | 20050 | 272 | −0.034 ±0.018 | $>22.0 (3\sigma)$ |
| U | 760 | 10 | 2.6 ±0.7 | $17.3^{+0.3}_{-0.2}$ | UVW2 | 24621 | 900 | −0.016 ±0.012 | $>22.1 (3\sigma)$ |
| U | 844 | 10 | 3.3 ±0.7 | $17.1^{+0.3}_{-0.2}$ | UVW2 | 37257 | 786 | −0.013 ±0.012 | $>21.9 (3\sigma)$ |
| U | 929 | 10 | 2.4 ±0.6 | $17.4^{+0.3}_{-0.2}$ | UVW2 | 48827 | 789 | −0.028 ±0.011 | $>23.6 (3\sigma)$ |
| U | 1149 | 100 | 1.9 ±0.2 | $17.6^{+0.1}_{-0.1}$ | White | 441766 | 10950 | 0.02 ±0.04 | $>21.9 (3\sigma)$ |
| U | 1775 | 100 | 1.4 ±0.2 | $18.0^{+0.1}_{-0.1}$ | White | 611955 | 3417 | −0.14 ±0.08 | $>22.3 (3\sigma)$ |
| U | 2401 | 100 | 1.0 ±0.1 | $18.3^{+0.2}_{-0.1}$ | White | 696516 | 3595 | −0.11 ±0.06 | $>22.6 (3\sigma)$ |
| U | 6723 | 900 | 0.47 ±0.04 | $19.2^{+0.1}_{-0.1}$ | White | 783075 | 5179 | −0.06 ±0.05 | $>22.3 (3\sigma)$ |
| U | 35498 | 900 | 0.17 ±0.04 | $20.3^{+0.3}_{-0.2}$ | White | 869866 | 4507 | −0.08 ±0.06 | $>22.1 (3\sigma)$ |
| U | 47066 | 900 | 0.11 ±0.04 | $20.8^{+0.5}_{-0.3}$ | White | 995723 | 3645 | −0.16 ±0.09 | $>22.2 (3\sigma)$ |
| UVW1 | 409 | 10 | 1.5 ±0.5 | $17.4^{+0.5}_{-0.3}$ | White | 1.21e+06 | 1712 | −0.10 ±0.14 | $>21.0 (3\sigma)$ |
| UVW1 | 494 | 10 | 1.6 ±0.5 | $17.3^{+0.4}_{-0.3}$ | | | | | |
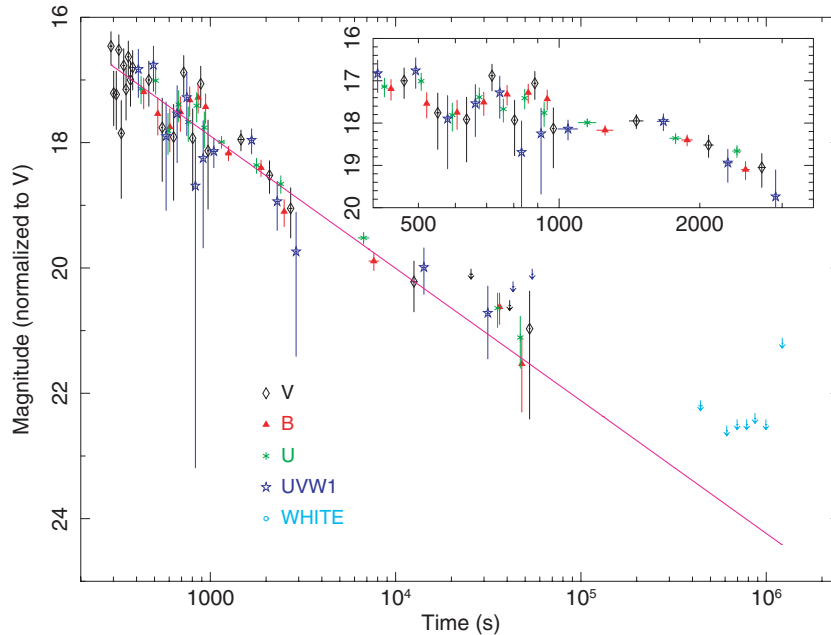
**Figure 1.** Optical light curve of GRB 050802 in four of the six filters available. The *UVM*2 and *UVW*2 filters were excluded from all plots as the data were not constraining. The count rates inside the 10-s exposures, between 400 and 1000 s were summed and averaged for each filter and the rest of the exposures were normalized against this value. The normalized count rate in each exposure was then divided by the average value for the *V* filter. Upper limits are given to $3\sigma$.

**Table 2.** For six UVOT filters, the normalization factor required to convert to *V* count rate. For *B*, *U*, *UVW*1, *UVM*2 and *UVW*2 filters, the normalization factor was calculated by taking the average count rate through the filter in the 400–1000 s range, and dividing this value by the average count rate in the *V* filter over the same time interval. The average count rates were then used to create an optical/UV SED, which was used to predict the ratio of white to *V* count rate.

| Filter | Ratio |
|--------|-------|
| *B* | 0.39 |
| *U* | 0.45 |
| *UVW*1 | 1.71 |
| *UVM*2 | 14.46 |
| *UVW*2 | 12.45 |
| White | 0.13 |

equivalent *V* count rates as follows. The optical–UV spectral energy distribution (SED) was modelled using the average count rates from the *V*, *B*, *U*, *UVW*1, *UVM*2 and *UVW*2 filters in the 400–1000 s time range. The optical/UV RMs were then used to predict the ratio of the *V* to white count rates.

### 3.3 Combined X-ray and UV/optical SEDs

SEDs were produced spanning the optical to X-ray range for early (400–1000 s) and late (35–55 ks) times. For each period, the average count rates of the exposures in each UVOT filter were used to produce the optical spectral values. For the X-ray part of each SED a spectrum was extracted in the relevant time range.

## 4 RESULTS

### 4.1 X-ray and optical light curves

The 0.2–10 keV X-ray light curve of GRB 050802 is shown in Fig. 2. A visual inspection shows a complex behaviour with an initial rise followed by a flat and then a more rapid decay. The X-ray light curve was first modelled using a broken power law. The best-fitting parameters were $\alpha_1 = 0.55 \pm 0.03$, $\alpha_2 = 1.59 \pm 0.03$ and break time $4600 \pm 260$ s. However, the $\chi^2/\text{d.o.f.} = 81/57$ corresponds to a null hypothesis probability of only 0.02, and the model systematically deviates from the observed light curve at the earliest times. Hence, the light curve was modelled using a double broken power law (i.e. a model with three power-law segments). This provides a better fit with $\chi^2/\text{d.o.f.} = 64/55$; according to the *F*-test the three-segment power-law fit gives an improvement at the $3\sigma$ confidence level with respect to the two-segment model. The values of the best-fitting parameters are shown in Table 3.

In the best-fitting model, the X-ray light curve first rises with a slope $\alpha_1 = -0.80^{+0.71}_{-0.35}$ until $420 \pm 40$ s. At this point, the light curve breaks for the first time and a shallow decay begins with $\alpha_2 = 0.63 \pm 0.03$. This phase ends at $5000 \pm 300$ s when the light curve starts to decay steeply with $\alpha_3 = 1.59 \pm 0.03$.

To look for spectral variations over the course of the decay, we split the light curve into soft (0.2–2 keV) and hard (2–10 keV) X-ray light curves. The soft and hard X-ray light curves are shown in Fig. 3, where we also show the softness ratio, which we define as $(C_S - C_H)/(C_S + C_H)$ where $C_S$ is the soft X-ray count rate and $C_H$ is the hard X-ray count rate. A constant can be fitted well through the softness ratio time series ($\chi^2/\text{d.o.f.} = 30/29$) revealing that there is no significant spectral evolution with time.

The optical light curve is shown in Fig. 1 and it is well fitted with a single power-law decay with a temporal index $\alpha_1 = 0.82 \pm 0.03$ ($\chi^2/\text{d.o.f.} = 71/63$). The light curve has no obvious colour evolution within the wavelength range of the UVOT over the duration of the burst afterglow.
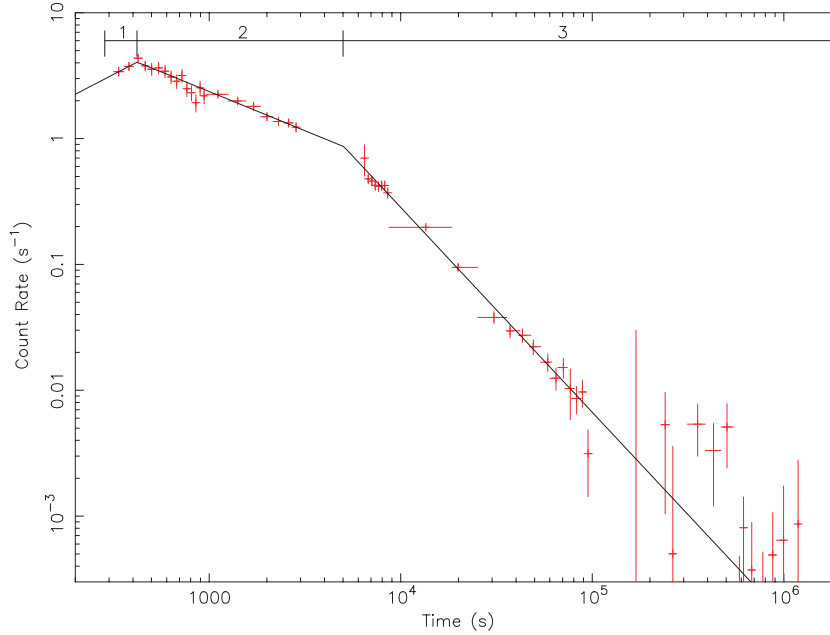
**Figure 2.** X-ray light curve of GRB 050802. A double broken power law is found to fit the X-ray light curve with breaks at $420 \pm 40$ and $5000 \pm 310$ s.

**Table 3.** Spectral and temporal analysis of the X-ray light curve of GRB 050802 fitted with three segments. The value of $N_H$ refers to the absorption at $z = 1.71$.

| Segment | Time at which slope breaks(s) | Energy index $\beta$ | $N_H(10^{20}\,\mathrm{cm}^{-2})$ | Temporal index $\alpha$ |
|---|---|---|---|---|
| 1 (initial rise) | $420 \pm 40$ | $0.87 \pm 0.08$ | $28 \pm 10$ | $-0.80^{+0.71}_{-0.35}$ |
| 2 (shallow decay) | $5000 \pm 300$ | $0.89 \pm 0.04$ | $31 \pm 5$ | $0.63 \pm 0.03$ |
| 3 (steep decay) | – | $0.88 \pm 0.04$ | $28 \pm 5$ | $1.59 \pm 0.03$ |

Fynbo et al. (2005a,b) observed an extended source within an arcsecond of the afterglow location, 1.5 d after the burst trigger. They suggested that it might be the host galaxy and they provided a combined magnitude for the afterglow and extended source of $R = 22.5$. We have looked for the host galaxy by co-adding the UVOT white filter images taken at late times after the afterglow has faded beyond detection. The UVOT white filter observations were taken until $1.2 \times 10^6$ s and are shown in Fig. 1. The summation of the white exposures provides a deep $3\sigma$ upper limit of 23.4 mag, which is equivalent to $V = 23.5$ mag for the afterglow spectrum. From these observations, we can confirm that there is no significant contribution from the host galaxy to the light curve in the UVOT spectral range for the first 60 ks, while the afterglow is still detected by the UVOT.

To determine the earliest time at which the optical light curve could have broken, a two-segment power law was fitted with the second segment decay rate set to be the same as the third segment in the X-ray light curve. We determined the $3\sigma$ lower limit for the break time by adjusting the time of the break until we obtained $\Delta\chi^2 = 9$ with respect to the single power-law fit. The lower limit to the break time was found to be 19 ks after the burst trigger, significantly later than the second X-ray break.

In Fig. 4 we show the X-ray/optical ratio, which we define as $(C_X - C_O)/(C_X + C_O)$ where $C_O$ is the optical/UV count rate normalized to the $V$ filter and $C_X$ is the X-ray count rate. Initially, we tried fitting a constant across the entire time range. This provided a poor fit with $\chi^2/$ d.o.f. $= 168/62$, implying that the changes in the

X-ray/optical ratio are highly significant. To investigate the behaviour of the X-ray/optical ratio we fit a function to it before and after the second X-ray break time of 5000 s. The first 5000 s was fitted by a linear relationship between $(C_X - C_O)/(C_X + C_O)$ and $\log(t)$ with a gradient of $0.24 \pm 0.01$ ($\chi^2/$d.o.f. $= 47/47$). After 5000 s, the best-fitting linear relationship has a $\chi^2/$ d.o.f. $= 7/12$ and gradient of $-0.09 \pm 0.01$. The evolving X-ray/optical ratio implies that the optical/UV to X-ray SED is changing throughout the afterglow.

### 4.2 X-ray and optical spectra

The results of the X-ray spectral analysis are shown in Table 3. All spectra were fitted using an absorbed power-law model. The absorption component includes both photoelectric absorption from our Galaxy and the host galaxy of the GRB. The Galactic column density was fixed at $N_H = 1.78 \times 10^{20}\,\mathrm{cm}^{-2}$ (Dickey & Lockman 1990) and the column density at $z = 1.71$ was allowed to vary. The spectral slopes and column densities measured for the three segments of the X-ray afterglow show no evidence of evolution. There is evidence for absorption from the host galaxy of the GRB in each segment; the column density is consistent between the three segments of the X-ray light curve, with an average value of $2.9 \times 10^{21}\,\mathrm{cm}^{-2}$.

Optical/UV to X-ray SEDs in the time intervals 400–1000 and 35–55 ks were created as described in Section 3.3. For each SED, a power-law fit accounting for Galactic and GRB host galaxy dust and
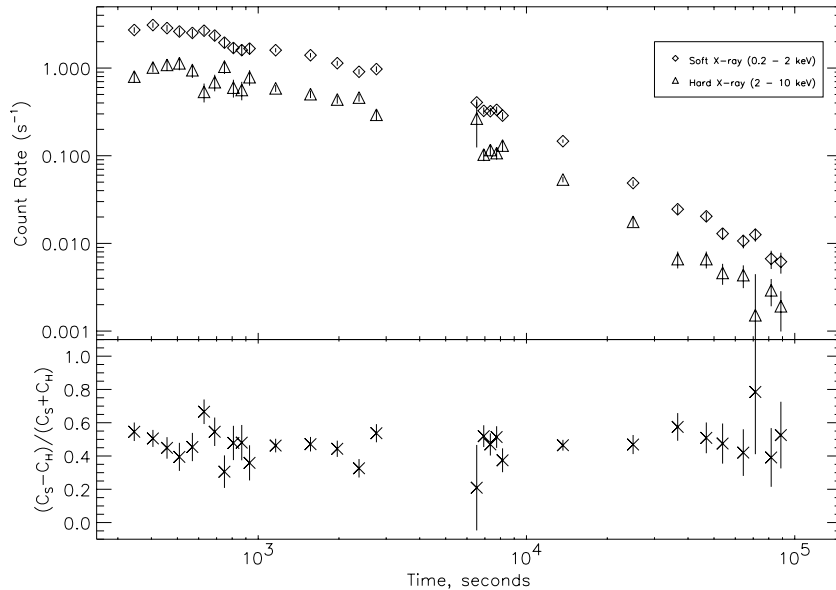
**Figure 3.** Top panel: the soft (0.2–2 keV) and hard (2–10 keV) X-ray light curves. Bottom panel: the softness ratio, defined as $(C_S - C_H)/(C_S + C_H)$, where $C_H$ is the hard X-ray count rate and $C_S$ is the soft X-ray count rate. There is no evidence for spectral evolution within this time period as can be seen by the constant ratio.
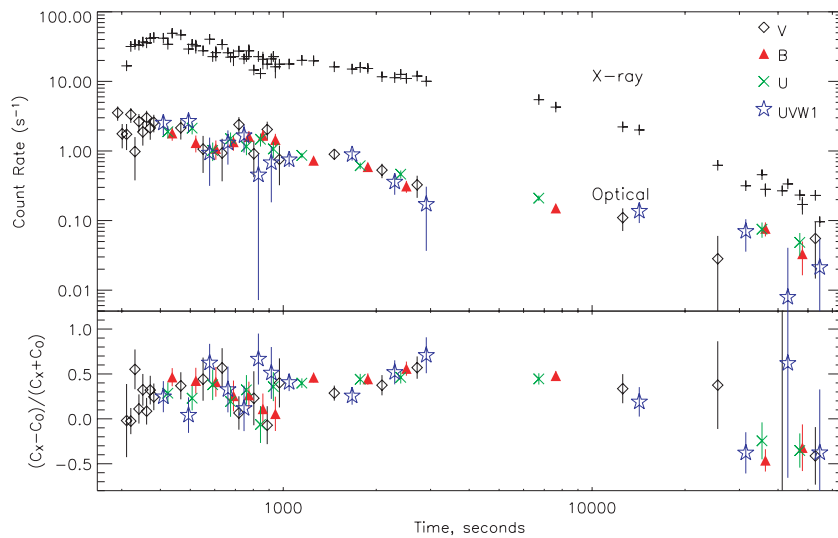


**Figure 4.** Top panel: the X-ray and optical light curves. The optical light curve is shown for four out of the six filters. The count rates in each filter have been normalized to the $V$ filter, as discussed the caption to Fig. 1. The X-ray light curve has been binned according to the length of each exposure in the optical light curve. Different symbols refer to the filters used for the optical observation in each time bin. Bottom panel: the ratio between the X-ray ($C_X$) and optical ($C_O$) light curves.

photoelectric absorption was applied (see Fig. 5). For extinction in our Galaxy, a fixed dust component was used with $E(B - V) = 0.03$, using the Milky Way (MW) extinction curve (Pei 1992). For extinction in the host galaxy the fit was tried using the Small Magellanic Cloud (SMC) extinction curve and then with the MW extinction curve. The fitting was applied to the 400–1000 s SED as these data have better signal-to-noise ratio than at late times. The fit using the SMC extinction curve produced $\beta = 0.79 \pm 0.02$ and $\chi^2$/ d.o.f. = 134/104. The fit using the MW extinction curve returned $\beta = 0.86 \pm 0.02$ and $\chi^2$/ d.o.f. = 120/104. We also tested a model in which a cooling break resides in between the optical and X-ray bands. In this case, a broken power-law model was tested in which the spec-

tral indices have a fixed difference of $\Delta\beta = 0.5$. For consistency, the model was tried using the SMC and MW extinction curves. The broken power law using the SMC extinction curve returned $E_{break} = 0.010^{+0.009}_{-0.008}$ keV and $\beta_2 = 0.89 \pm 0.01$ with $\chi^2$/d.o.f. = 125/103. The fit using the MW extinction curve gave $E_{break} = 0.004^{+0.005}_{-0.003}$ and $\beta_2 = 0.89 \pm 0.04$ with $\chi^2$/d.o.f. = 119/103. Overall, the fits with the MW extinction curve provide the best $\chi^2$/d.o.f. and for this extinction curve there is no significant improvement to the fit by replacing a power law with a broken power law. The model parameters from the different model fits and the implied total (Galactic and GRB host galaxy) extinction in the UVOT bands are given in Table 4.
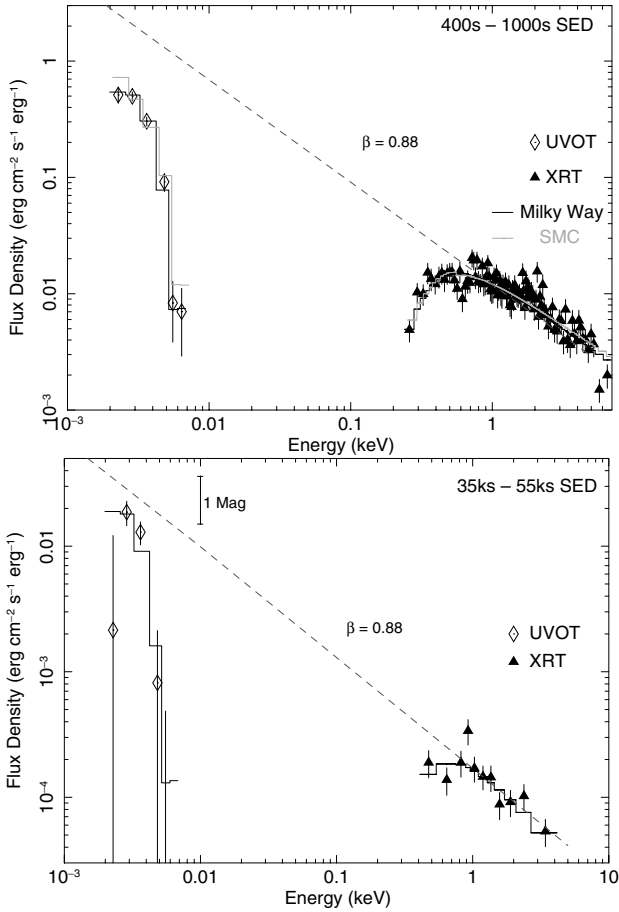
**Figure 5.** Optical and X-ray SEDs between 400 and 1000 s (top) and 35–55 ks (bottom). The top panel shows the fit using SMC dust extinction (grey; offset by a factor of 1.1) and MW extinction (black). The first six points in each panel show the six filters of the UVOT ranging from *V* to *UVW*2. Points after 0.2 keV show the X-ray spectrum from 0.2 to 10 keV. In the top and bottom panels, the dashed line represents the weighted mean of the spectral indices found in the three segments of the X-ray light curve, $\beta = 0.88$.

Unusually, we find that the MW extinction curve best fits the SED of GRB 050802. In comparison, no other bursts in the samples of Schady et al. (2007) or Starling et al. (2006), which consist of seven *Swift* GRBs and 10 *BeppoSAX* GRBs, respectively, are fitted best with an MW extinction curve. Since the extinction curve is unusual, we determined the $N_H/A_V$ to see how this compares to other GRBs. For GRB 050802, the $N_H/A_V$ ratio was found to be $4.5(\pm 2.3) \times 10^{21}$. The mean GRB $N_H/A_V$ ratio for an MW extinction law in the sample of Schady et al. (2007) is $4.7^{+1.4}_{-1.3} \times 10^{21}$, so GRB 050802 is consistent with the mean $N_H/A_V$ in Schady et al. (2007) to within $1\sigma$. This implies that the ratio of dust and gas surrounding GRB 050802 is fairly typical for GRBs.

Because we have shown that the absorption does not change significantly with time, we do not expect the extinction to change either. Therefore, in fitting the 35–55 ks SED we froze the extinction and absorption at the best-fitting values found for the 400–1000 s SED. This resulted in a fit with $\beta = 0.99 \pm 0.02$ ($\chi^2$/ d.o.f. = 27/15), which implies a null hypothesis of only 3 per cent. Furthermore, the value of $\beta$ obtained in this fit is inconsistent at 99 per cent confidence with $\beta_3 = 0.88 \pm 0.04$, the spectral index of the third segment of the X-ray light curve. If we repeat the fit to the 35–55 ks SED with

a fixed spectral index of $\beta = 0.88$, we obtain a $\chi^2$/d.o.f. = 35/16, which implies the model is rejected at 99 per cent confidence.

## 5 DISCUSSION

In summary, we have determined that the X-ray light curve can be divided into three segments with two breaks at 420 and 5000 s. Throughout the afterglow, there is no evidence for X-ray spectral evolution. We also find that the optical light curve decays as a single power law, which has a slightly steeper decay than the second segment of the X-ray light curve. We have determined the earliest possible time that the optical light curve could have changed its decay rate to match that of the third X-ray segment to be 19, which is 14 ks after the last X-ray break.

In the following subsections, we will look in detail at the X-ray afterglow to examine the origin of the X-ray breaks and to determine the best-fitting closure relations between the temporal and spectral slopes. Then we shall discuss the question of why the X-ray light curve breaks at 5000 s while the optical light curve continues to decay as a power law. Several mechanisms will then be investigated to find a compatible model for the production of the X-ray and optical afterglow.

### 5.1 The X-ray afterglow

We begin by looking at the first break to see what we may learn. The break occurs at $420 \pm 40$ s, which is preceded by a rise from 286 s with a slope of $-0.80^{+0.71}_{-0.35}$. The break is then followed by a gradual decay with a slope of $\alpha = 0.63 \pm 0.03$. The rise and the successive slow decay can be regarded as a broad peak in the light curve and it may be attributed to 'flaring' activity (Burrows et al. 2005b; Nousek et al. 2006) or could be the early phase of the jet interacting with the external medium, giving rise to the forward shock (Kumar & Piran 2000a). However, it is not possible to discriminate between the two mechanisms. Flares often have different spectra to the afterglow, but if this is a flare it may be so small we would not expect to see any spectral variability. On the other hand, we cannot tell if this is the early rise of the afterglow as we have too little data prior to the peak. An additional contribution to the second segment from a large flare may also be excluded as a power-law fit to the X-ray light curve between 1000- and 3000-s results in a slope of $\alpha = 0.64 \pm 0.05$ with $\chi^2$/ d.o.f. = 21/38.

Typically, X-ray afterglows are analysed by applying the closure relations given by Zhang et al. (2005) to the X-ray spectral and temporal indices. These relations are an aid in determining the location of the observed X-ray band relative to the synchrotron frequencies ($\nu_a$, $\nu_m$, $\nu_c$) and the environment in which the burst occurs.

We skip the first segment of the X-ray light curve as the closure relations are not applicable to a light curve that is rising. We begin by applying the simplest non-injected relations to the second segment, in which $\alpha_2 = 0.63 \pm 0.03$ and $\beta_2 = 0.89 \pm 0.04$, the only closure relation that agrees without the requirement of energy injection at $3\sigma$ confidence level, is

$$\alpha = \frac{3\beta - 1}{2}. \tag{1}$$

This relation applies to a wind or interstellar medium (ISM) with $\nu_X > \nu_c$, but, this relation is not appropriate for GRB 050802 as the value of the energy index $p$, determined through $\beta = p/2$ is $p = 1.78 \pm 0.08$. Values of $p < 2$ require a different set of closure relations provided by Zhang & Mészáros (2004), of which none

**Table 4.** The model parameters were determined from the fitting of a power law and separately a broken power law to the 400–1000 s SED; the fits were repeated for the MW and SMC extinction curves. Also shown is the power law with MW extinction fit to the 35–55 ks SED. Parameters marked with * are fixed at the best-fitting values found for the power-law fit to the 400–1000 s using MW extinction. All models use a fixed value of the Galactic extinction $E(B-V) = 0.03$ and Galactic absorption $N_{\rm H} = 1.78 \times 10^{20}\,{\rm cm}^{-2}$. The observed host extinction in each filter is provided for each fit; note that these were derived from the fit parameter $E(B-V)_{\rm host}$ and were not fit parameters in their own right.

| Model parameters and host extinction | Models for 400–1000 s SED | | | | 35–55 ks SED |
| --- | --- | --- | --- | --- | --- |
| | Power-law MW extinction | Power-law SMC extinction | Broken power-law MW extinction | Broken power-law SMC extinction | Power-law MW extinction |
| $\beta$ | $0.86 \pm 0.02$ | $0.79 \pm 0.02$ | $0.89 \pm 0.04$ | $0.89 \pm 0.01$ | $0.99 \pm 0.02$ |
| Energy $_{\rm break}$ (keV) | – | – | $0.004^{+0.005}_{-0.003}$ | $0.010^{+0.009}_{-0.008}$ | – |
| $E(B-V)_{\rm host}$ | $0.18 \pm 0.02$ | $0.09 \pm 0.01$ | $0.18 \pm 0.02$ | $0.10 \pm 0.02$ | $0.18^*$ |
| $N_{\rm H_{host}}(\times 10^{20}\,{\rm cm}^{-2})$ | $26 \pm 4$ | $20 \pm 4$ | $29 \pm 6$ | $30 \pm 4$ | $26^*$ |
| $A_V$ (mag) | $1.6 \pm 0.2$ | $0.8 \pm 0.1$ | $1.6 \pm 0.2$ | $0.8 \pm 0.1$ | $1.6^*$ |
| $A_B$ (mag) | $1.4 \pm 0.2$ | $1.2 \pm 0.1$ | $1.5 \pm 0.2$ | $1.1 \pm 0.1$ | $1.4^*$ |
| $A_U$ (mag) | $1.7 \pm 0.2$ | $1.4 \pm 0.2$ | $1.8 \pm 0.2$ | $1.4 \pm 0.2$ | $1.7^*$ |
| $A_{UVW1}$ (mag) | $2.5 \pm 0.3$ | $1.8 \pm 0.2$ | $2.6 \pm 0.3$ | $1.8 \pm 0.3$ | $2.5^*$ |
| $A_{UVM2}$ (mag) | $2.8 \pm 0.3$ | $1.9 \pm 0.2$ | $2.9 \pm 0.3$ | $1.9 \pm 0.3$ | $2.8^*$ |
| $A_{UVW2}$ (mag) | $2.8 \pm 0.3$ | $1.9 \pm 0.2$ | $2.9 \pm 0.3$ | $1.9 \pm 0.3$ | $2.8^*$ |
| $\chi^2$/ d.o.f. | 120/104 | 134/104 | 119/103 | 125/103 | 27/15 |

satisfies the second decay of GRB 050802. More complex closure relations, which include a third parameter to account for energy injection, are provided by Zhang et al. (2005). In these models the luminosity is assumed to evolve as $L(t) = L_0(t/t_{\rm b})^{-q}$ where $q$ is the luminosity index and $t_{\rm b}$ is the time for the formation of a self-similar solution, which is approximately the deceleration time. The luminosity index $q$ must be $<1$ for the energy injection to affect the afterglow dynamics. We found that there are two injected closure relations that are consistent with $\alpha_2$ and $\beta_2$. The first relation is

$$\alpha = \frac{q}{2} + \frac{(2+q)\beta}{2}. \tag{2}$$

This closure relation is for a wind medium with slow cooling electrons with either $\nu_{\rm X} < \nu_{\rm m}$ or $\nu_{\rm m} < \nu_{\rm X} < \nu_{\rm c}$ and where $q = -0.27 \pm 0.04$. The second possible energy-injected relation is

$$\alpha = (q-1) + \frac{(2+q)\beta}{2}. \tag{3}$$

This relation is for a uniform medium with slow cooling electrons with either $\nu_{\rm m} < \nu_{\rm X}$ or $\nu_{\rm m} < \nu_{\rm X} < \nu_{\rm c}$ and where $q = 0.51 \pm 0.04$. For the closure relations given in equations (2) and (3), $\beta = (p-1)/2$ and so $p = 2.79 \pm 0.08$.

When the closure relations are applied with the indices of the third segment, where $\alpha_3 = 1.59 \pm 0.03$ and $\beta_3 = 0.88 \pm 0.04$, we find that the most consistent closure relation without energy injection is

$$\alpha = \frac{3\beta + 1}{2}, \tag{4}$$

which is consistent at $3.5\sigma$ confidence. All other non-injected closure relations are ruled out at a minimum of $4\sigma$. Equation (4) is for electrons that are slow cooling within the range $\nu_{\rm m} < \nu_{\rm X} < \nu_{\rm c}$ in a wind medium. Again a value for the energy index may be determined though $\beta = (p-1)/2$ with $p = 2.76 \pm 0.08$. Generally, the energy index is expected to remain constant throughout the X-ray afterglow, unless it is changed by energy injection (Zhang et al. 2005).

Therefore, the application of the closure relations to the X-ray temporal and spectral indices suggests that the second segment is energy injected and the third segment is not, and therefore that the break between the second and third segments at $\simeq 5000$ s is due to the discontinuation of energy injection. At this point it is worth

pointing out that the second and third segments of GRB 050802 are consistent with the second and third segments of the canonical light curve presented by Nousek et al. (2006). Furthermore, from the application of the closure relations above we would come to the same physical explanation as Nousek et al. (2006) and Zhang et al. (2005) for this temporal behaviour: that the break between the two segments corresponds to the end of energy injection. Having looked at the X-ray afterglow in isolation, we will now investigate whether this physical picture is compatible with the observed optical emission. The standard afterglow is based on the assumption of a single relativistic outflow (Mészáros & Rees 1997a) and we will begin by considering models of this type before considering multicomponent outflows.

### 5.2 Can the X-ray and optical afterglow be explained by a single jet?

We start by considering an afterglow in which the emission in both the X-ray and optical bands is produced predominantly by the forward shock. If we compare the decay of the optical light curve with the segments of the X-ray light curve we find that the optical decay is similar, although not identical to, the slow 'energy-injected' decay of the second segment. This would suggest that the optical light curve is also characteristic of an energy-injected afterglow. Since the X-ray light curve breaks at 5000 s, suggesting the end of energy injection, and the optical light curve continues with a shallow decay indicative of energy injection, we first consider the possibility that the electrons responsible for producing the optical emission continue to receive energy while the X-ray emitting electrons do not.

There are two possible mechanisms for continued energy injection. These are the arrival of additional shells of material at the shock region or the release of energy stored in the form of Poynting flux. In the first case, the injected energy changes the fireball dynamics, but can only change the balance of X-ray to optical emission and produce a break in one of the light curves if $\nu_{\rm m}$ or $\nu_{\rm c}$ pass through one of these bands. However, we can rule out the passage of one of these breaks through the X-ray or optical afterglow because there is no break in the optical light curve and there is no change in the

X-ray spectrum. This therefore rules out continued energy in the form of blast waves and so we consider continued energy injection in the form of Poynting flux. Energy is supplied in the form of Poynting flux when there is a rotating compact object that has a magnetic field, $B$. The flux is converted to kinetic energy when kink instabilities cause the magnetic field lines to reconnect in the outflow (Drenkhahn 2002; Giannios & Spruit 2006). The energy density of Poynting flux is $\propto B^2$, and within the reconnection region the energy available per particle for particle acceleration is $\propto B$ (Giannios 2006). To decrease the photon energy so that further emission is below the X-ray band, requires a decrease of the average particle energy. The XRT is sensitive over more than a decade in photon energy, therefore a decrease in the average photon energy from above the XRT energy band to below the XRT energy band requires a factor of $>10$ change in $B$ and therefore a factor of $>100$ change in the energy density of Poynting flux (Giannios 2006). This implies a large change in the overall rate of energy injection, which is inconsistent with the continued power-law decay in the optical.

A reverse shock is an alternative means for producing optical emission without X-ray emission and so we now examine the possibility that this could sustain the optical emission of GRB 050802 after the X-ray light curve has broken. The reverse shock will travel back through the ejected matter and will emit as long as it is passing through ejecta. The reverse shock emission will cease when it passes over the last ejected shell (Zhang & Mészáros 2002). The shock crossing time is expected to be approximately the duration of the GRB, but if energy continues to be injected into the afterglow by the arrival of further shells the reverse shock may continue for as long as the energy injection phase. If the end of energy injection occurs at 5000 s, as suggested by the X-ray light curve, then we should expect that the reverse shock must cease at approximately 5000 s. Therefore, this is not the required mechanism as the optical light curve has no break until at least 19 ks.

Panaitescu et al. (2006a) have proposed that it is possible to sustain a power-law decay in the optical, while the X-ray light curve shows a break due to the end of energy injection, if the microphysical parameters are changing with time. The microphysical parameters that must change to keep the optical temporal decay as a power law are: the fraction of post-shock energy in the magnetic fields $\epsilon_B$, the fraction of post-shock energy that is given to electrons $\epsilon_i$ and the blast-wave kinetic energy $E$ (Nousek et al. 2006; Panaitescu et al. 2006a). These parameters are expected to evolve with Lorentz factor $\Gamma$, if they evolve at all. In the scenario proposed by Panaitescu et al. (2006a), the cooling frequency $\nu_c$ lies between the optical and X-ray bands. In this case, there should be a slope change of $\Delta\beta = 0.5$ between the X-ray and optical bands and $\nu_c$ moves to lower frequencies with time (Panaitescu et al. 2006a). For GRB 050802, through the fitting of a broken power law with a fixed $\Delta\beta = 0.5$ to the 400–1000 s SED (see Section 4.2), the maximum energy, at which a break could be present, was determined to be 0.02 keV.

We examined the optical to X-ray SEDs to see if the X-ray and optical light curves can be explained by $\nu_c$ moving to lower frequencies with time as expected in the model of Panaitescu et al. (2006a). In this model the largest change in the ratio $(C_X - C_O)/(C_X + C_O)$, where $C_X$ is the X-ray count rate and $C_O$ is the *V*-band count rate corresponds to the motion of $\nu_c$ from its highest allowed value to below the optical passband, at which point the optical emission lies on the same power-law spectral segment as the X-ray emission. In the broken power-law fit to the 400–1000 s SED, the highest allowed value of $\nu_c$ at $3\sigma$ confidence is 0.06 keV. Therefore we refitted the 400–1000 s SED with $\nu_c$ fixed at 0.06 keV, then reduced the value

of $\nu_c$ to below the UVOT spectral range and so determined that the smallest $(C_X - C_O)/(C_X + C_O)$ value allowed by this model is $-0.10$. The observed range of $(C_X - C_O)/(C_X + C_O)$ extends to much lower values than this (Fig. 4). We find that the weighted mean of the data points more than 35 ks after the BAT trigger is $(C_X - C_O)/(C_X + C_O) = -0.38 \pm 0.08$, which is $>3\sigma$ below the lowest allowed value of $-0.10$, thus allowing the model of Panaitescu et al. (2006a) to be ruled out.

We now look into the optical to X-ray SED further and ask: to what extent can single-component models be ruled out completely? As discussed in Section 4.2, a power-law fit to the late time (35–55 ks) SED provides a poor fit and the best-fitting value of $\beta$ is softer than the X-ray spectral index for segment 3, which includes the 35–55 ks time interval. In this respect, we note that there is no evidence for any evolution in the X-ray spectral index at any point in the afterglow and the weighted mean of the indices found in the three segments of the X-ray light curve gives $\beta = 0.88 \pm 0.03$. To see why the fit to the late-time SED is poor we show the X-ray spectrum extrapolated to lower energies using this spectral slope ($\beta = 0.88$) as a dashed line in both panels of Fig. 5. The dashed line lies above the optical and UV data points as expected for an afterglow with significant extinction. In Section 4.2, we determined that at $3\sigma$ confidence, the host galaxy extinction is greater than 0.8 and 1.1 in the $B$ and $U$ bands, respectively, no matter which models we choose for the extinction and continuum. In addition, the Galactic extinction is 0.1 for both the $B$ and $U$ bands. After correction for extinction, the $B$- and $U$-band fluxes in the late-time SED lie significantly above the dashed line. As described in Section 4.2, this power law can be ruled out with $>99$ per cent confidence, implying at 99 per cent confidence that the region responsible for the X-ray emission cannot produce all of the optical emission at late times, no matter where $\nu_c$ and $\nu_m$ lie. Since single-component outflows are unable to represent the late-time SED satisfactorily, we now consider multicomponent outflows to see which of these models are able to reproduce the observed light curves and SEDs.

### 5.3 Multicomponent outflows

A multicomponent outflow is one consisting of two or more components that have different bulk Lorentz factors. The simplest model is one of two components: a narrow jet and a second wider, but slower jet that surrounds the narrow component. This geometry may be generated by the narrow jet giving rise to a wider and slower component (Kumar & Granot 2003), where the bulk $\Gamma$ decreases over time and produces a jet with angular structure. Alternatively, the two components may be formed at the same time, for example, when neutrons and protons decouple in a neutron-rich, hydroydynamically accelerated jet from a neutron star or from the neutron-rich accretion disc of a collapsed massive star (Vlahakis et al. 2005). Peng et al. (2005) show that within such a neutron-rich jet, the wide component has greater energy than the narrow component so that the wider component is able to dominate at late times. In both cases, the narrow component will produce the X-ray emission, whereas the optical emission will be produced by the wider component as it travels at lower Lorentz factors than the narrow component. This picture can be used to explain bursts such as GRB 021004 and GRB 030329 (Peng et al. 2005). The wider jet is expected to reach the undisturbed medium at a slightly later time than the narrow jet. Thus, the wide component may be observed as a later start for the optical light curve when compared to the X-ray light curve, or on an established optical light curve, the arrival of the wide jet to the

external medium may be shown as a late rise/bump or a change in the decay slope.

There are three options within a two-component jet we will investigate to see if one could have produced the observed light curves of GRB 050802. All of these options involve energy injection, which is introduced through shells of material. The options are: energy injection with the ejected shells wide enough to refresh both components of the jet with a Lorentz factor that decreases over time (so that after 5000 s the shells no longer reach the shock in the narrow component), the cessation of energy injection at 5000 s in one component only and, finally, the continuation of energy injection for the duration of the afterglow, but with the narrow component producing a jet break at 5000 s.

The first option is that energy injection is distributed uniformly throughout both jets and continues for a sustained period of time. Initially, the shells have a wide enough angular distribution, and travel at a $\Gamma$ large enough, to reach the forward shock produced by both components. Both the X-ray and the optical afterglows will appear energy injected. As time goes by, the Lorentz factor of the freshly ejected shells decreases. Eventually, the ejected shells will not travel at a Lorentz factor large enough to reach the shocked region in the narrow component, but will still be able to reach the wide component. This will cause a break to be seen only in the X-ray afterglow. However, the freshly ejected shells will still travel at $\Gamma$ large enough to reach the wide component and therefore the optical light curve will continue to appear energy injected. This much appears to be consistent with the data because, as discussed in Section 5.2, the optical light curve appears to be energy injected for its entire observed duration and does not break with the X-ray light curve. However, as the wide component is slower than the narrow component, the wide component will absorb shells (i.e. receive energy) at a faster rate than the narrow component. Therefore, the optical emission is expected to decay less rapidly than the X-ray emission. For GRB 050802, the opposite is actually observed: in the optical the decay index $\alpha_O = 0.82 \pm 0.03$, while the X-ray second segment has a decay index of $\alpha_2 = 0.63 \pm 0.03$, thus this model is excluded.

The second option calls for the X-ray break at 5000 s to have been caused by the cessation of energy injection in the narrow component, while injection continues in the wide component. However, this implies that the energy is injected as a hollow jet at late times and we consider this to be an unattractive solution on physical grounds, and lacking in testable predictions.

The third option is that energy is continuously injected into both components and the X-ray break at 5000-s results from a jet break of the narrow component (Panaitescu & Kumar 2004). The spectral indices of the X-ray segments support this model as there is no spectral change over the break, as is expected for a jet break. A jet break may be produced within a laterally expanding or a non-expanding jet. The closure relations for these cases are provided by Panaitescu et al. (2006b). In order for this scenario to be viable we have to find a post-jet-break closure relation that has consistent energy injection, external medium, synchrotron frequencies and electron spectral index to that of the pre-jet-break closure relation. The closure relation that satisfies this uses equation (3)5 of Panaitescu et al. (2006a), and is

$$\alpha = (1 + 2\beta) - \frac{2}{3}(1 - q)(\beta + 2). \qquad (5)$$

This relation is independent of the GRB host medium and is for a laterally expanding jet with $\nu_m < \nu < \nu_c$. The relation provides a value of $q = 0.38 \pm 0.04$, which is consistent at the 99 per cent confidence level with the value of $q$ obtained through the closure

relation in equation (3). The consistency with equation (3) implies that this burst originated in a uniform ISM and not a wind medium as suggested in Section 5.1.

Furthermore, we can use the second X-ray break time to infer the opening angle of the narrow beam and to put a lower limit on the angle of the wide component. We calculated the angles using the following expression from Frail (2001):

$$\theta_{jet} = 0.057 t_{jet}^{3/8} \left(\frac{1+z}{2}\right)^{-3/8} \left(\frac{0.2E_{iso}}{\eta}\right)^{-1/8} \left(\frac{n}{0.1}\right)^{1/8}, \qquad (6)$$

where $E_{iso}$ is the isotropic energy of the burst, $n$ is the density of the medium and $\eta$ is the efficiency of converting energy in the ejecta into $\gamma$-rays. We use values of $E_{iso} = 0.2 \times 10^{53}$ erg (in the range 15–350 keV) and GRB efficiency $\eta = 0.2$. Approximating the circumburst medium as a spherical, uniform gas cloud of radius $R$, the particle density $n$, may be estimated simply as $n = N_H/R$. The cloud radius for gas and dust to survive the GRB, may be estimated using fig. 8 of Perna & Lazzati (2002). This shows that the obscuring medium must extend to $R \sim 10^{20}$ cm, implying a number density of $n \sim 30$ cm$^{-3}$. Thus, the value for the narrow component is estimated to be $\theta_{jet,narrow} \sim 1°$ and for the wide component the opening angle is $\theta_{jet,wide} \geqslant 8°$. We recognize that these angles are only approximate because they depend weakly on the bolometric energy, the efficiency of the burst and on the particle density of the external medium.

This model requires that energy be continually injected into both components of the jet for the observed duration of the burst. The time-scale over which this energy injection takes place is more than an order of magnitude larger than $10^3$–$10^4$ s, which is the duration of energy injection required to explain the canonical X-ray afterglow (Zhang et al. 2005; Capalbi et al. 2006; Krimm et al. 2006; Nousek et al. 2006; Tashiro et al. 2006). This situation may seem unusual, but GRB 050802 is not the first burst that has required discrete or continuous energy injection for an extended period. A few examples of bursts that have required long duration energy injection are GRB021004, XRF050406 and GRB060729 (Björnsson, Gudmundsson & Jóhannesson 2004; Grupe et al. 2006; Romano et al. 2006). The continuation of energy injection well beyond the jet break time will produce shallower post jet break slopes than the non-injected case and these may be mistaken for the discontinuation of energy injection. This would lead to the surprisingly small number of reported jet breaks in the *Swift* era (Willingale et al. 2006). However, the mechanism that could be responsible for long duration ($>10^4$ s) energy injection is uncertain. Currently, the most favoured scenario is one in which the duration of the central engine is short, but where the ejecta are emitted with shells of varying velocities (Rees & Mészáros 1998). The shells will order themselves before reaching the external medium and will form a continuous flow of shells. In this case, small time-scale fluctuations need not be observed in the power-law light curves and the central engine is not required to be particularly long lived.

This model would allow the break to occur only in the X-ray light curve because the narrow and wide components travel at different $\Gamma$, and the narrow component is beamed into a smaller angle. Therefore, the two-component outflow with continued energy injection and a jet break in the narrow component is our favoured hypothesis for producing the observed light curve of GRB 050802.

The result from this paper has wider implications for our understanding of GRBs. Segments 2 and 3 of the X-ray light curve of GRB 050802 have the same characteristics as the segments 2 and 3 of the canonical X-ray afterglow light curve (Nousek et al. 2006). If we had looked at the X-ray data alone, then our explanation for the

second and third X-ray segments of GRB 050802 would have been equivalent to the explanation proposed by Nousek et al. (2006) and Zhang et al. (2005) for the canonical light curve: an energy-injected decay followed by a 'normal' decay. However, when the optical observations are taken into account, this explanation is no longer attractive. Instead, a more plausible explanation is a two-component outflow with the break in the X-ray light curve likely to be due to a jet break. Our results suggest that without the optical light curve the interpretation of GRB afterglows may not be correct.

## 6 CONCLUSION

This paper has investigated GRB 050802, an unusual burst because the optical decays as a power law, while the X-ray breaks twice. We have analysed optical and X-ray data gathered from the XRT and UVOT instruments onboard *Swift*. Observations continued with both the XRT and the UVOT up until $1.2 \times 10^6$ s.

The analysis of the afterglow began by looking at the origin of the three power-law segments in the X-ray light curve. The X-ray light curve commences with a rise until 420 s. The second segment decays slowly with $\alpha_2 = 0.63 \pm 0.03$ until 5000 s. The third and last segment decays faster with a slope of $\alpha_3 = 1.59 \pm 0.03$. The optical light curve decays as a single power law with $\alpha_O = 0.82 \pm 0.03$.

Through modelling of the 400–1000 s X-ray to optical SED, it was determined that the best fit is a power law with MW extinction. However, when extinction in the host galaxy is accounted for, the optical points lie above the X-ray power law at late times, indicating that the optical afterglow could not be produced by the same component as the X-ray emission. This result rules out single-component afterglows with 99 per cent confidence.

The next logical step was to examine a multicomponent outflow. Several variations of a two-component jet, the simplest multicomponent outflow, were investigated. Of all the possibilities, we find the most physically self-consistent model is one in which both a narrow and a wide component are energy injected for the duration of the observed afterglow and the X-ray break at 5000 s is due to a jet break in the narrow component.

This paper has wide implications for the GRB community. We have found that the explanation obtained by examining only the X-ray data of GRB 050802 differs remarkably from the answer obtained by examining the optical and X-ray emission together. Our results suggest that without the optical light curve the correct interpretation of GRB afterglows may not be possible.

## ACKNOWLEDGMENTS

## REFERENCES

Band D. et al., 2005, GCN Circ., 3734
Bathelmy S. D. et al., 2005, Space Sci. Rev., 120, 143
Björnsson G., Gudmundsson E. H., Jóhannesson G., 2004, ApJ, 615, L77
Burrows D. N. et al., 2005a, Space Sci. Rev., 120, 165
Burrows D. N. et al., 2005b, Sci, 309, 1833
Capalbi M. et al., 2006, A&A, 462, 913
Dai Z. G., Lu T., 1998a, A&A, 333, L87
Dickey J. M., Lockman F. J., 1990, ARA&A, 28, 215
Drenkhahn G., 2002, A&A, 386, 714
Frail D. A., 2001, ApJ, 562, L55
Fynbo J. U. et al., 2005a, GCN Circ., 3749
Fynbo J. U. et al., 2005b, GCN Circ., 3756
Giannios D., 2006, A&A, 455, L5
Giannios D., Spruit H. C., 2006, A&A, 450, 887
Grupe D. et al., 2006, ApJ, 662, 443
Krimm H. A. et al., 2006, ApJ, 648, 1117
Kumar P., Piran T., 2000a, ApJ, 532, 286
Kumar P., Granot J., 2001, ApJ, 591, 1075
McGowan K., Band D., Brown P., Gronwall C., Huckle H., Hancock B., 2005, GCN Circ., 3739
Mészáros P., Rees M. J., 1997, ApJ, 476, 232
Nousek J. A. et al., 2006, ApJ, 642, 389
Palmer D. et al., 2005, GCN Circ., 3737
Panaitescu A., Kumar P., 2004, MNRAS, 350, 213
Panaitescu A., Mészáros P., Gehrels N., Burrows D., Nousek J., Gehrels N., O'Brien P., Willingale R., 2006a, MNRAS, 369, 2059
Panaitescu A., Mészaros P., Gehrels N., Burrows D., Nousek J., 2006b, MNRAS, 366, 1357
Pavlenko E., Efimov Y., Shylapnikov A., Baklanov A., Pozanenko A., Ibrahimov M., 2005, GCN Circ., 3744
Pei C., 1992, ApJ, 394, 130
Peng F., Königl A., Granot J., 2005, ApJ, 626, 966
Perna R., Lazzati D., 2002, ApJ, 580, 261
Rees M. J., Mészáros P., 1998, ApJ, 496, L1
Romano P. et al., 2006, A&A, 450, 59
Roming P. et al., 2005, Space Sci. Rev., 120, 95
Sari R., 1997, ApJ, 489, 37
Sari R., Piran T., 1997, ApJ, 585, 270
Sari R., Piran T., Helpen J. P., 1999, ApJ, 519, L17
Schady P. et al., 2007, MNRAS, 377, 273
Starling R. L. C. et al., 2006, ApJ, 661, 787
Tashiro M, S. et al., 2006, PASJ (Suzaku Special Issue), 59, S361
Vlahakis N., Peng F., Königl A., 2003, ApJ, 594, L23
Willingale R. et al., 2006, ApJ, 662, 1093
Zhang B., Kobayashi S., 2005, ApJ, 628, 315
Zhang B., Mészáros P., 2001, ApJ, 552, L35
Zhang B., Mészáros P., 2002, ApJ, 566, 712
Zhang B., Mészáros P., 2004, Int. J. Mod. Phys. A, 19, 2385
Zhang B., Fan Y. Z., Dyks J., Kobayashi S., Mészaros P., Burrons D. N., Nousek J. A., Gehrels N., 2006, ApJ, 642, 354

This paper has been typeset from a TEX/LATEX file prepared by the author.